RMetS
Royal Meteorological Society

# Maintenance mechanisms for the early-morning maximum summer rainfall over southeast China

Wan-Ru Huang* and Johnny C. L. Chan

*Guy Carpenter Asia-Pacific Climate Impact Centre, School of Energy and Environment, City University of Hong Kong, China*
*Correspondence to: Wan-Ru Huang, Guy Carpenter Asia-Pacific Climate Impact Centre, School of Energy and Environment, City University of Hong Kong, Tat Chee Ave., Kowloon, Hong Kong, China.
E-mail: wrhuang@cityu.edu.hk

**During the summer months, diurnal rainfall variation over southeast China is frequently characterized by a major peak in the afternoon and a minor peak in the early morning. While the afternoon rainfall maximum is generally recognized to be mainly modulated by the diurnally varying wind introduced by land–sea and mountain–valley differential heating, causes of the early-morning rainfall are not well documented. In this study, variation in the semi-diurnal harmonic of rainfall is found to be more important than variation in the diurnal harmonic of rainfall for determining the timing of the early-morning rainfall peak. Diagnoses of the atmospheric thermodynamic conditions indicate that late-night vertical differential thermal advection and semi-diurnal variation in land–sea differential radiative heating/cooling are the major reasons for reduction in stability in the early morning and, in turn, facilitate the formation of an early-morning maximum in rainfall. Computation of the water vapor budget suggests further that the early-morning maximum over southeast China is mainly maintained by the semi-diurnal harmonic of water vapor flux transported from the South China Sea.** 

*Key Words:* semi-diurnal variation; atmospheric heat budget; water vapor budget

*Received 2 June 2010; Revised 03 January 2011; Accepted 23 February 2011; Published online in Wiley Online Library*

*Citation:* Huang W-R, Chan JCL. 2011. Maintenance mechanisms for the early-morning maximum summer rainfall over southeast China. *Q. J. R. Meteorol. Soc.* DOI:10.1002/qj.815

## 1. Introduction

East Asia (hereafter, EA), with complex mountain–valley and land–sea distributions, exhibits large regional differences in the times of occurrence of maximum diurnal precipitation, particularly during the summer months (June, July, and August, or JJA) (Dai, 2001; Zhao *et al.*, 2005, 2008; Kikuchi and Wang, 2008). For stations located west of 110°E, diurnal rainfall in the summer tends to peak at midnight or in the early morning (Asai *et al.*, 1998; Wang *et al.*, 2004; Yu *et al.*, 2007a; Li *et al.*, 2008). Such a feature also predominates in some areas east of 110°E, including the middle and lower reaches of the Yangtze River, the North China Plain, and the coastal regions of China (Peacock, 1952; Chan and Ng, 1993; Yin *et al.*, 2009; Chen *et al.*, 2010). In contrast, the northern and southern parts of areas east of 110°E are dominated by daytime precipitation (Chen *et al.*, 1999, 2009; Yu *et al.*, 2007a). Because the diurnal rainfall over EA varies with a high geographical dependence, many previous studies (e.g. Wai *et al.*, 1996; Yu *et al.*, 2007b; Chen *et al.*, 2010) have been undertaken to understand the physical mechanisms involved in forming the different timing of maximum diurnal rainfall. A detailed review for many of these previous proposed mechanisms can be found in Yang and Smith (2006).

In summer, the low-level southwesterly monsoon winds bring warm and moist air from the South China Sea to EA and generate heavy rainfall there (see Zhou and Chan, 2005 and Figure 1(a)). Modulated by the diurnally varying monsoon circulation, large hour-to-hour rainfall variability is revealed over southeast China (SEC; boxed area in

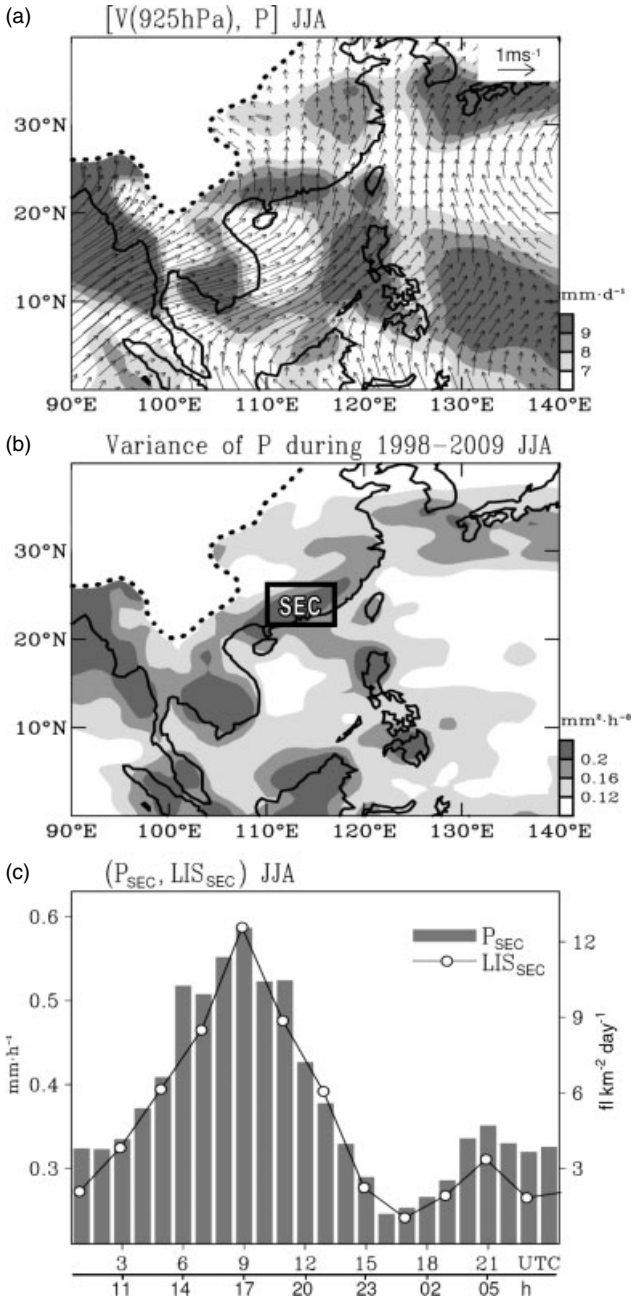


**Figure 1.** (a) Summer (June, July, and August; JJA) mean of 925 hPa wind vector superimposed with precipitation (shaded). (b) Variance of hourly precipitation during the 1998–2009 summer periods. The color scale of (a, b) is shown at right bottom and mountain areas in (a, b) are blocked. (c) Temporal variations of JJA mean hourly precipitation ($P$; histogram; scale on left ordinate, in fl km$^{-2}$ day$^{-1}$) and 2-hourly lightning activities (LIS; solid line with open circles; scale on right ordinate) area-averaged over southeast China (SEC; 110$^-$118°E, 21$^-$25°N; boxed area in (b)). Local time in SEC is universal time (UTC) + 8 h.

Figure 1(b)). It was noted from rain gauge observations that the hourly rainfall over SEC (hereafter, $P_{SEC}$) frequently consists of two peaks within a day (e.g. Ramage, 1952; Yin *et al.*, 2009). Generally, a major maximum peak of $P_{SEC}$ occurs in the afternoon and a minor maximum peak appears in the early morning (Figure 1(c)). Such an afternoon rainfall maximum was generally attributed to moist convection connected with solar heating (e.g. Chen *et al.*, 1999; Dai, 2001). In contrast, causes of the early-morning maximum $P_{SEC}$ have rarely been discussed and are not well documented.

To produce the early-morning maximum $P_{SEC}$, there should be other mechanisms different from the daily solar heating, which disappears at night, for initiating a relatively unstable atmospheric thermodynamic condition in the early morning. Previous studies investigating the possible causes of nocturnal rainfall over the Yangtze River region, the coastal region of China (e.g. Hong Kong), and an island near SEC (e.g. Taiwan) found that nocturnal instability over these areas can be initiated by diurnally varying low-level atmospheric thermal advection (e.g. Ramage, 1952; Chen *et al.*, 2010), radiative cooling at the top of the cloud (e.g. Gray and Jacobson, 1977; Chen *et al.*, 2010), and convergence of surface wind and water vapor flux (e.g. Wai *et al.*, 1996; Chen *et al.*, 1999). Here, we propose that all these mechanisms have impacts on the formation of the early-morning maximum $P_{SEC}$ as well.

The periodic incoming solar heating in the atmosphere generates global tidal waves which can be revealed from variables such as pressure, wind, temperature, and even precipitation. The tidal waves evolve with periods of 24 and 12 h and are commonly referred to as the diurnal and semi-diurnal oscillations respectively (e.g. Wallace and Hartranft, 1969; Hamilton, 1980; Deser and Smith, 1998; Yin *et al.*, 2009). Because the semi-diurnal harmonic component of $P_{SEC}$, i.e. S2$(P)_{SEC}$, consists of two peaks including one in the early morning (explained later in Figure 2(c)), we further hypothesize that the physical mechanisms involved for the formation of S2$(P)_{SEC}$ are important and non-negligible for the occurrence of an early-morning maximum $P_{SEC}$.

The main objective of this study is to examine these hypotheses, which are important because a proper conceptual model for the formation of early-morning maximum $P_{SEC}$ and S2$(P)_{SEC}$ that contributes ∼30% of the total variability of $P_{SEC}$ within a day (explained later in Figure 2(c)) can have significant implications regarding the improvement of weather and climate simulations over SEC. Analyses are performed based on data introduced in section 2. Results are presented in sections 3–5, followed by a summary in section 6.

## 2. Data and methodology

The analyses utilize meteorological data extracted from the 3-hourly GEOS5 (Goddard Earth Observing System Model Version 5; Rienecker *et al.*, 2008) reanalyses because it gives a higher sampling rate for both the diurnal and semi-diurnal harmonics than other 6-hourly reanalyses (Dai and Deser, 1999; Chen, 2005). The spatial resolution of GEOS5 is 0.667° longitude × 0.5° latitude (about 66.7 km in longitude × 50 km in latitude, a scale smaller than that of a typical local land–sea breeze ∼100 km) which provides a good depiction of the regional diurnal wind variation (Huang *et al.*, 2010). The precipitation analysis uses the TRMM (Tropical Rainfall Measuring Mission; Simpson *et al.*, 1996) 3G68 2B31 dataset because it uses both passive and active microwave data to produce the best rain estimate for TRMM (Haddad *et al.*, 1997a, 1997b), which has been shown to resemble rain gauge observations, with a good representation of the diurnal rainfall variability (Hong *et al.*, 2005; Zhou *et al.*, 2008; Chen *et al.*, 2009). In addition, lightning activities extracted from the TRMM LIS/OTD Climatology production (hereafter, LIS) are also examined. The spatial and temporal resolutions of TRMM-3G68, LIS

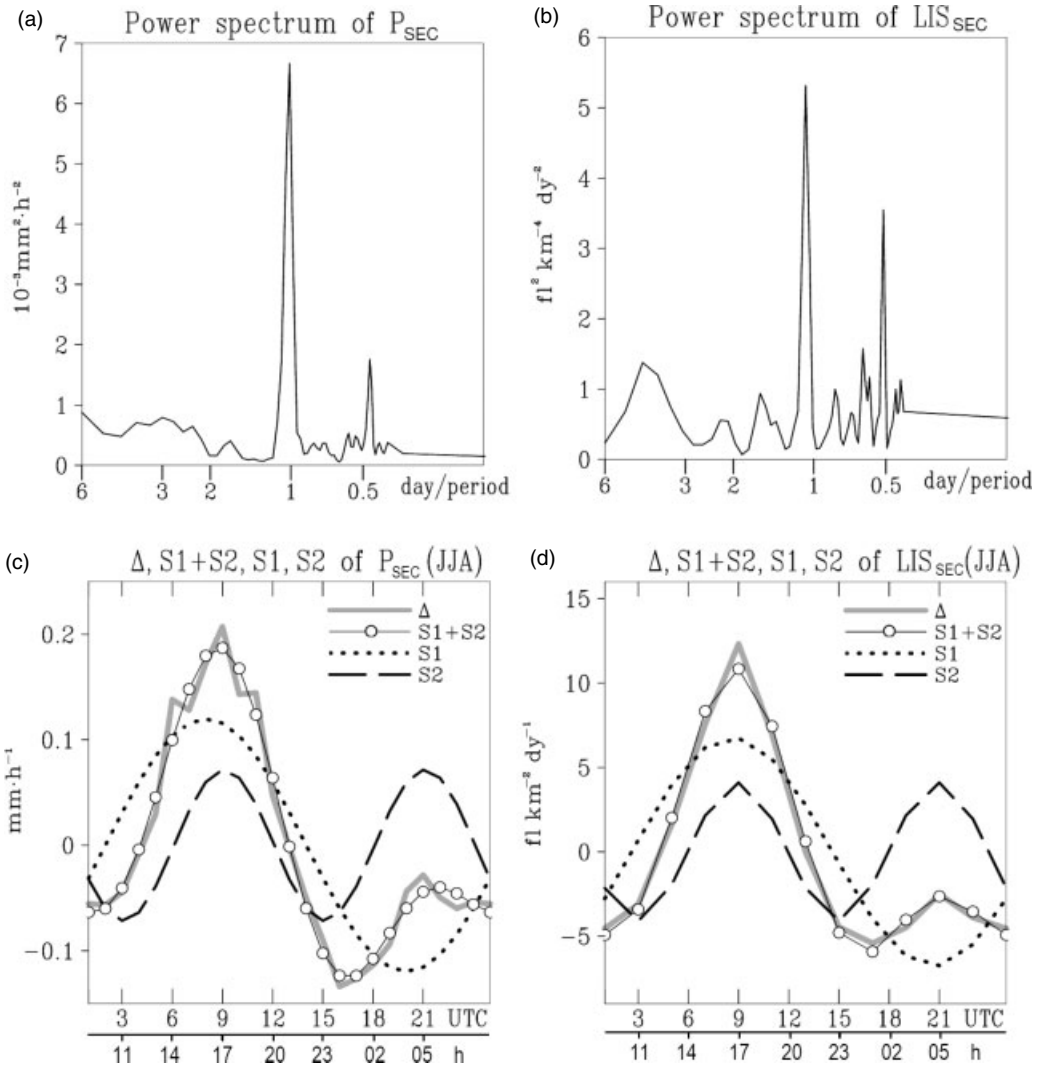


**Figure 2.** Power spectrum analyses of (a) hourly precipitation over SEC, i.e. $P_{SEC}$, and (b) 2-hourly lightning activity over SEC, i.e. $LIS_{SEC}$, during the 1998–2009 summer periods. (c) Temporal variations of JJA mean hourly $P_{SEC}$ anomalies (Δ: thick grey solid line) and its associated diurnal harmonic (S1: dotted line), semi-diurnal harmonic (S2; long dash line), and a combination of diurnal and semi-diurnal harmonics (S1 + S2; thin solid line with open circles). (d) Similar to (c), but for the temporal variations of $\Delta LIS_{SEC}$ and its related harmonic modes.

are 0.5° × 0.5°, 0.5° × 0.5° respectively and 1-hourly, 2-hourly respectively. The time period of study is summer from 1998 to 2009 (June, July, and August).

In this study, SEC is defined as an area covering (110–118°E, 21–25°N). Kikuchi and Wang (2008) identified three different rainfall regimes based on the amplitude, peak time, and phase propagation characteristics of diurnal precipitation. Here we note from a longitude–time diagram of rainfall averaged between 21°N and 25°N (not shown) that the area between (110–115°E, 21–25°N), which shows no or only a little landward phase propagation, can be identified as the continental rainfall regime based on Kikuchi and Wang's (2008) definition. The rest of the SEC area (115–118°E, 21–25°N) belongs to the coastal rainfall regime, with a large portion of landward phase propagation and a very small portion of seaward phase propagation. Kikuchi and Wang (2008) suggested that the maximum rainfall over the continental regime occurs in the afternoon (1500–1800 h) and over the landward coastal regime from noon to evening (1200–2100 h). Consistent with this suggestion, it is shown in Figure 1(c) that the maximum $P_{SEC}$ occurs at 1700 h.

Hereafter, local time in SEC is universal time (UTC) + 8 h, e.g. 0800 h is 0000 UTC. Anomalies of a given variable at a specific synoptic time step (e.g. 0000 UTC) are computed by subtracting the daily means from available hourly observations. The diurnal and semi-diurnal harmonic components of anomaly variables are obtained by Fourier analysis. The anomalies, diurnal (i.e. first harmonic) and semi-diurnal (i.e. second harmonic) cycles of a given variable $X$ are denoted by $\Delta X$, S1($X$) and S2($X$), respectively.

## 3. General characteristics of diurnal variations over SEC

It is clear from Figure 1(c) that the summer hourly precipitation area-averaged over SEC, i.e. $P_{SEC}$, has a primary maximum value in the afternoon at 1700 h (universal time 0900 UTC), a minimum value during 0000–0100 h (1600–1700 UTC), and a minor peak in the early morning at 0500 h (2100 UTC). Such a temporal evolution is also revealed in the lightning activities area-averaged over the same domain ($LIS_{SEC}$; Figure 1(c)), confirming the times of the occurrence of two rainfall peaks. Power spectrum analyses of $\Delta P_{SEC}$ and $\Delta LIS_{SEC}$ variations during the 1998–2009 summer periods also show the diurnal and semi-diurnal

as the two dominant oscillation periods (Figure 2(a) and (b) respectively). Yin *et al.* (2009) suggested that the hourly rainfall records from 62 selected rain gauges over China can be well explained by their S1 and S2 harmonics with a 90% confidence threshold. Consistent with Yin *et al.* (2009), it is found that ∼97% and 98% of the variance of $\Delta P_{\mathrm{SEC}}$ and $\Delta \mathrm{LIS}_{\mathrm{SEC}}$ respectively (thick grey solid line in Figure 2(c) and (d) respectively) is explained by the variance of their combining S1 and S2 harmonics (thin solid line with open circles). In addition, it is also noted from Figure 2(c) and (d) that the variance of $\mathrm{S2}(P)_{\mathrm{SEC}}$ and $\mathrm{S2(LIS)}_{\mathrm{SEC}}$ contributes to ∼30% and 35% of the variance of $\Delta P_{\mathrm{SEC}}$ and $\Delta \mathrm{LIS}_{\mathrm{SEC}}$ respectively.

As seen from Figure 2(c), the occurrence of afternoon rainfall maximum over SEC is mainly determined by the variation in $\mathrm{S1}(P)_{\mathrm{SEC}}$, which has a maximum value at 1700 h and a minimum value at 0500 h. In contrast to $\mathrm{S1}(P)_{\mathrm{SEC}}$, the maximum value of $\mathrm{S2}(P)_{\mathrm{SEC}}$ appears at both 1700 and 0500 h. The variation of $\mathrm{S2}(P)_{\mathrm{SEC}}$ therefore likely plays an important role in affecting the formation of two rainfall peaks in Figure 1(c). In other words, if the contribution of $\mathrm{S2}(P)_{\mathrm{SEC}}$ to $\Delta P_{\mathrm{SEC}}$ is ignored, the magnitude of primary rainfall peak at 1700 h is underestimated and there is no minor rainfall peak at 0500 h. Despite its importance, physical mechanisms responsible for causing $\mathrm{S2}(P)_{\mathrm{SEC}}$ have rarely been discussed, as compared to that for producing $\mathrm{S1}(P)_{\mathrm{SEC}}$. This is probably due to a concern that the temporal resolution of the reanalysis data used by previous studies (e.g. Li *et al.*, 2008; Chen *et al.*, 2009) is generally 6-hourly, which might not be adequate for depicting the S2 signal.

To explain the variation of $\Delta P_{\mathrm{SEC}}$, characteristics of the atmospheric dynamical and thermal conditions varying within a day are studied. Dynamically, the low-level diurnal wind variation, which can be estimated from the JJA mean of 925 hPa wind anomalies denoted by $\Delta[\mathbf{V}(925\ \mathrm{hPa})]$ at four selected synoptic time steps (Figure 3(a)), is an important factor in affecting the diurnal rainfall variation (Deser and Smith, 1998; Dai and Deser, 1999). Yu *et al.* (2009) investigated the wind anomalies over central eastern China and proposed that the anomalous wind vectors exhibit clockwise rotation diurnally, as shown in Figure 3(a), which is likely related to the formation of a low-level jet that helps the generation of the nocturnal rainfall in the Yangtze River region (Chen *et al.*, 2010). Because land has a smaller specific heat capacity than sea, solar heating during the daytime (e.g. 1700 h/0900 UTC) tends to make the atmosphere over land warmer than that over the ocean (e.g. Figure 3(b)), whereas radiative cooling during the night leads to the former being cooler than the latter (not shown). Huang *et al.* (2010) noted that such a land–sea differential heating during the daytime helps the introduction of a local sea breeze along the EA coastline which apparently couples with the global-scale diurnal atmospheric pressure tidal wave and, in turn, forms a planetary-scale sea breeze-like circulation over EA and the western North Pacific (Figure 3(b); see also Huang *et al.*, 2010).

The large-scale sea breeze-like circulation shown in Figure 3(b) is found to be dominated by its diurnal component (not shown), which explains more than 80% of the total variability of the zonal wind speed, based on the spatial variance of $\mathrm{S1}[u(925\ \mathrm{hPa})]$ divided by that of $\Delta[u(925\ \mathrm{hPa})]$ over the entire domain of Figure 3(b). The spatial distribution of $\mathrm{S1}[\mathbf{V}(925\ \mathrm{hPa})]$ at 1700 h (0900 UTC; Figure 3(b)) can further lead to strong low-level convergence into SEC (Figure 3(c)), matching well with the occurrence of maximum $\mathrm{S1}(P)_{\mathrm{SEC}}$ in the afternoon. Further evidence regarding the atmospheric thermodynamic condition in response to the cause of the afternoon rainfall peak over SEC is revealed from $\mathrm{S1}(\partial\theta_e/\partial p)$, the diurnal mode of moist static instability induced by the vertical differential of equivalent potential temperature $\theta_e$. As seen from Figure 3(d), the areas with positive $\mathrm{S1}(\partial\theta_e/\partial p)$ are distributed over SEC, indicating an unstable environment with active ascending motion suitable for the occurrence of an afternoon rainfall maximum over SEC at 1700 h (e.g. Huang *et al.*, 2010).

Because the characteristics of the S1 harmonic of atmospheric thermodynamic conditions over SEC at 1700 h (Figure 3(c) and (d)) are opposite to those observed at 0500 h (2100 UTC; Figure 3(e) and (f)), other forcing mechanisms different from the solar heating must exist to make the environment relatively unstable at 0500 h compared with other hours without solar heating in order to produce the early morning peak of $P_{\mathrm{SEC}}$. As seen from Figure 3(a), SEC is located on the east side of the Tibetan Plateau, where the enhancement of southerly wind anomalies appears at 0200 h (i.e. 1800 UTC) before the formation of the early-morning rainfall peak. The diurnally varying low-level thermal advection therefore likely plays a role in affecting the early-morning instability over SEC, as hypothesized earlier. To verify this argument, a diagnosis of the atmospheric heat budget is performed next.

## 4. Diagnosis of atmospheric heat budget

A typical heat budget equation can be expressed as (e.g. Wei *et al.*, 1983; Holton, 1992)

$$\underbrace{\frac{\partial T}{\partial t}}_{\mathrm{DT}} = \underbrace{\frac{\dot{Q}}{c_{\mathrm{p}}}}_{\mathrm{DIA}} + \underbrace{\sigma\omega}_{\mathrm{VA}} + \underbrace{(-\mathbf{V}\cdot\nabla T)}_{\mathrm{HA}} \tag{1}$$

where $\mathbf{V}$, $T$, $\sigma$, $\omega$, $\dot{Q}$ and $c_{\mathrm{p}}$ are the horizontal wind velocity, atmospheric temperature, static stability, p-vertical velocity, diabatic heating, and specific heat with constant pressure. Equation (1) consists of a temperature tendency term (DT), a diabatic heating term (DIA), a vertical thermal advection term (VA), and a horizontal thermal advection term (HA). Using these terms, temperature variations at a specific time step can be reconstructed by integrating Eq. (1):

$$T = \int_{t-3h}^{t} [\mathrm{DIA} + \mathrm{VA} + \mathrm{HA}]\, \mathrm{d}t = T^{\mathrm{DIA}} + T^{\mathrm{VA}} + T^{\mathrm{HA}} \tag{2}$$

where $T^{\mathrm{DIA}}$, $T^{\mathrm{VA}}$, and $T^{\mathrm{HA}}$ represent temperature changes induced by the DIA, VA, and HA terms respectively. With the temporal resolution of GEOS5, a 3 h time interval is used in Eq. (2) for the time integration.

Based on Eq. (1), the anomalies, S1, and S2 harmonics of three heating terms (i.e. DIA, VA, and HA) are computed to study the changes in atmospheric thermal condition within a day. The VA and HA terms are calculated directly from the GEOS5 reanalysis data, whereas the DIA term is obtained as a residual (Chen *et al.*, 2010). According to Eq. (2), the atmospheric thermal condition over SEC in the early morning at 0500 h/2100 UTC can be inferred from the variations of three heating terms at 0200 h/1800 UTC. It is found that over SEC at 1800 UTC the amplitude of

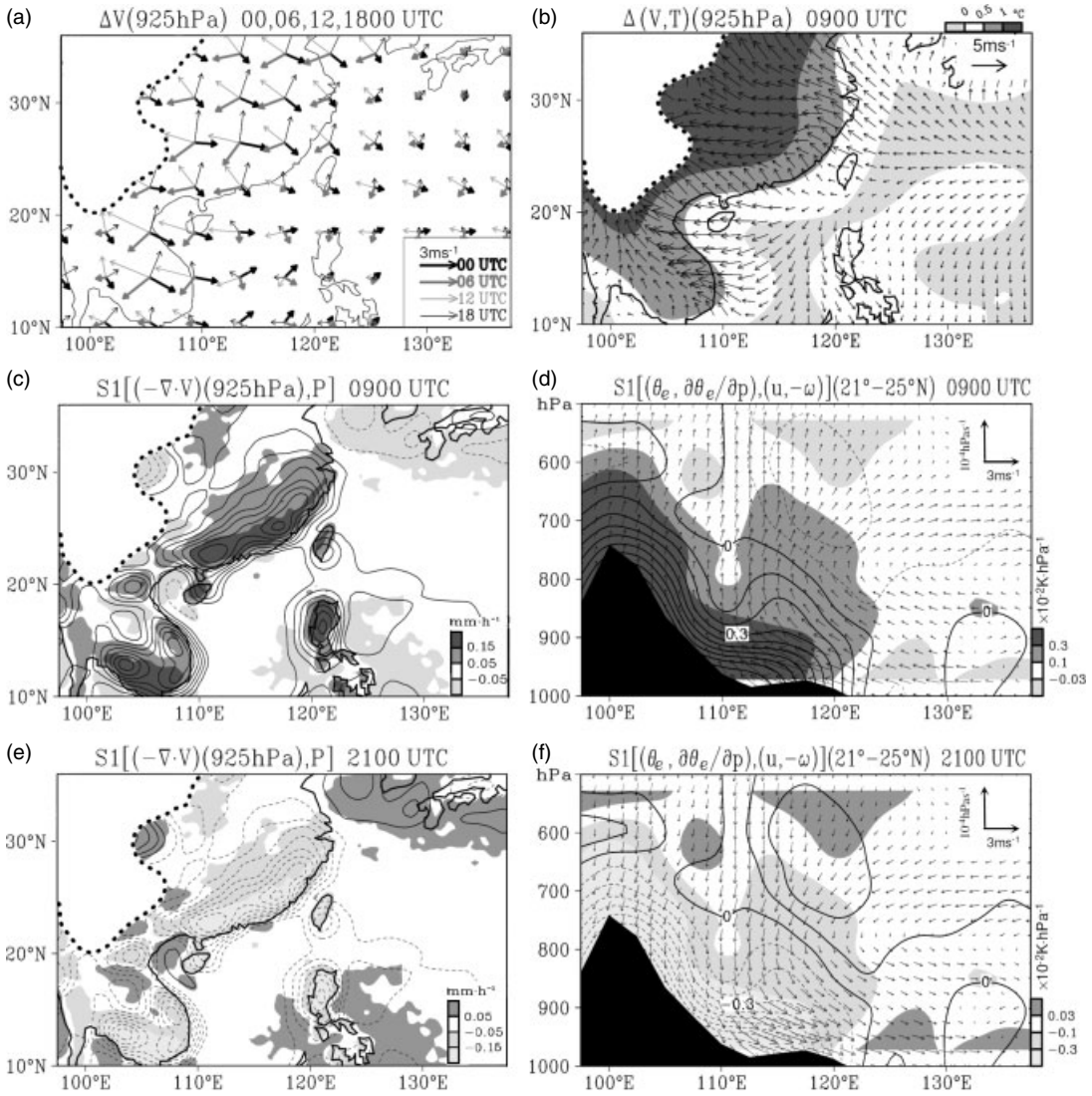


**Figure 3.** (a) JJA mean of 925 hPa wind anomalies at four selected time steps: 0000, 0600, 1200, and 1800 UTC. (b) Anomalies of 925 hPa wind (vectors) and temperature (shaded) at 0900 UTC (i.e. 1700 h for SEC). (c) S1 harmonic of 925 hPa wind convergence, i.e. S1$(-\nabla \cdot \mathbf{V})$, superimposed with S1$(P)$ at 0900 UTC. (d) Longitude–height cross-section of S1 harmonic of equivalent potential temperature, i.e. S1$(\theta_e)$ (contours), superimposed with S1$(\partial\theta_e/\partial p)$ (shaded) and S1$(u, -\omega)$ (vectors) averaged between 21°N and 25°N at 0900 UTC. The color scale of (b) and (c, d) is given at top right and bottom right, respectively. The contour interval of (c) and (d) is $5 \times 10^{-6}$ s$^{-1}$ and 0.1°C. (e) and (f) are similar to (c) and (d) respectively but for the 2100 UTC (i.e. 0500 h for SEC).

S1[VA(925 hPa)] (Figure 4(b)) and S1[HA(925-hPa)] (Figure 4(c)) are two orders larger than their related S2 harmonics (not shown). For this reason, only the S1 harmonics of three heating terms at 1800 UTC are presented in Figure 4(a)–(c) for a detailed discussion. The S2 harmonic of the DIA term is discussed in section 5.

It can be inferred from Figure 4(a) and Eq. (2) that the variations in S1[DIA(925 hPa)] at 1800 UTC would decrease the low-level atmospheric temperature over SEC at 2100 UTC, i.e. S1$(T^{\mathrm{DIA}})_{\mathrm{SEC}} < 0$. Examples of diabatic processes related to the changes in S1[DIA(925-hPa)] include solar or terrestrial radiation and the release of latent heat (Holton, 1992). In contrast with Figure 4(a), low-level warm air advection with positive values of S1[HA(925 hPa)] is revealed over SEC (Figure 4(c)), implying an increase in atmospheric temperature at 2100 UTC, i.e. S1$(T^{\mathrm{DIA}})_{\mathrm{SEC}} > 0$. Such a positive S1[HA(925 hPa)] over SEC appears at 1800 UTC when land is cooler than sea and the wind with strong southerly wind speed is flowing from the warmer South China Sea (hereafter, SCS) to the cooler SEC, whereas the values of S1[HA(925 hPa)] over the SCS are negative (Figure 4(c)) because not only is heat being advected away from this region towards the SEC but also there is some advection from the cooler Indochina Peninsula to the SCS.

A comparison between Figure 4(a)–(c) indicates that the impact of S1[VA(925 hPa)] on the early-morning temperature change over SEC can be ignored because it is at least one order of magnitude smaller than the other two heating terms. Among Figure 4(a)–(c), S1(HA) seems to be the one which is able to reduce the early-morning atmospheric stability caused by S1(DIA). This argument is clarified further by examining the temporal evolution of multi-level S1(HA) area-averaged over SEC (i.e. S1$(\mathrm{HA})_{\mathrm{SEC}}$; Figure 4(d)). It is noted that the occurrence of maximum low-level warm air advection is in conjunction with the occurrence of an upper-level cold air advection at 1800 UTC (Figure 4(d)). Such a low-level warming and upper-level cooling feature implies that thermal stability at 2100 UTC is reduced by the diurnally varying thermal advection at 1800 UTC.

 

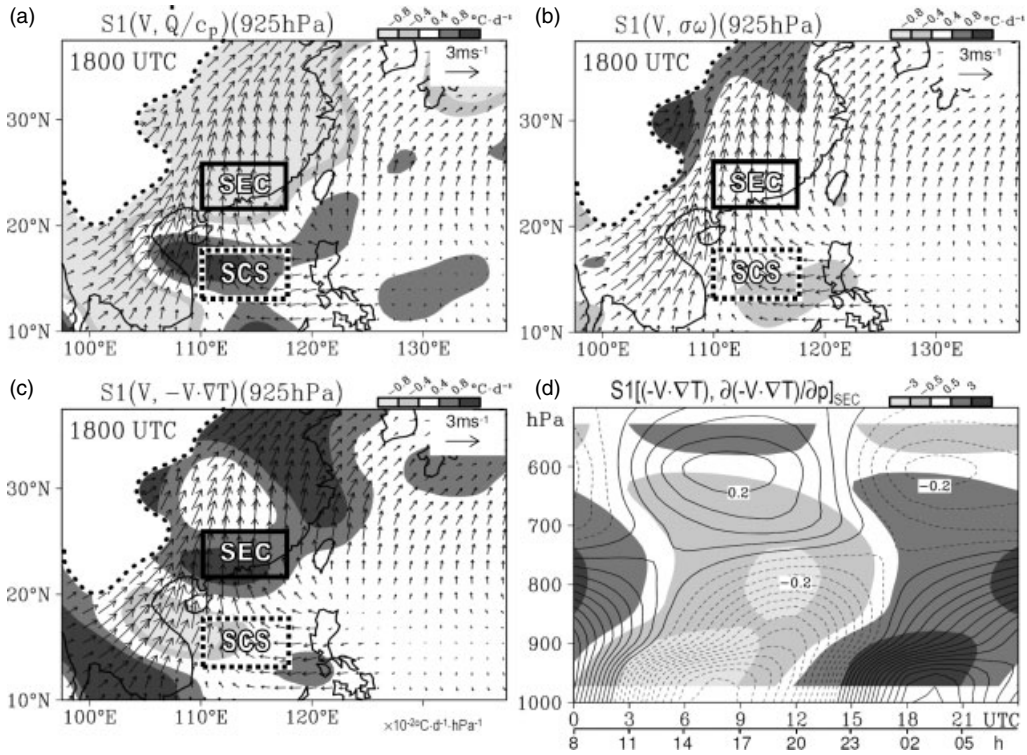


**Figure 4.** JJA mean of diurnal harmonic of 925 hPa heat budget analysis at 1800 UTC (i.e. 0200 h for SEC): (a) diabatic heating term S1($\dot{Q}/c_p$), (b) vertical advection of temperature term S1($\sigma\omega$), and (c) horizontal thermal advection term S1($-\mathbf{V}\cdot\nabla T$). The wind vectors of S1[$\mathbf{V}$(925 hPa)] at 1800 UTC are added in (a)–(c). (d) Temporal–vertical evolution of S1($-\mathbf{V}\cdot\nabla T$) (contours) and S1[$\partial(-\mathbf{V}\cdot\nabla T)/\partial p$] (shaded) area-averaged over SEC. The domain of SEC and SCS is denoted by boxed areas in (a)–(c). The color scale of (a)–(d) is given at top right. The contour interval of (d) is 0.1°C d$^{-1}$.

In addition to the diurnally varying thermal advection which affects S1($T^{\mathrm{HA}}$), variations in cloud radiative heating/cooling and water vapor convergence are two other hypothsized mechanisms for causing the early-morning rainfall over SEC. Analogous to Eq. (1), the atmospheric temperature change over SEC in the early morning is rewritten as

$$\begin{aligned}\Delta T &= \mathrm{S1}(T) + \mathrm{S2}(T)\\ &= \mathrm{S1}(T^{\mathrm{DIA}}) + \mathrm{S1}(T^{\mathrm{HA}}) + \mathrm{S1}(T^{\mathrm{VA}})\\ &\quad + \mathrm{S2}(T^{\mathrm{DIA}}) + \mathrm{S2}(T^{\mathrm{HA}}) + \mathrm{S2}(T^{\mathrm{VA}})\\ &\approx \mathrm{S1}(T^{\mathrm{DIA}}) + \mathrm{S1}(T^{\mathrm{HA}}) + \mathrm{S2}(T^{\mathrm{DIA}}) \qquad (3)\end{aligned}$$

In Eq. (3), the contributions of S1($T^{\mathrm{VA}}$), S2($T^{\mathrm{VA}}$), and S2($T^{\mathrm{HA}}$) to $\Delta T$ at 2100 UTC are ignored based on a scale analysis. It is known that radiative heating/cooling is one of the major diabatic processes included in the DIA term (Holton, 1992). As inferred from Eq. (3) and Figure 2(c), the hydrological circulation change in response to the S1 harmonic of radiative heating/cooling should be important to the formation of afternoon rainfall maximum over SEC, whereas that in response to the S2 harmonic of radiative heating/cooling might be important in affecting early-morning rainfall peak over SEC. Evidence supporting this argument are presented in the next section.

## 5. Diagnosis of hydrological cycle–radiation interaction

Several processes including radiative heating/cooling, associated change of static stability, and land–ocean processes that have been proposed in the published literature as mechanisms for the early-morning maximum in rainfall were documented in Yang and Smith (2006). Gray and Jacobson (1977) examined possible causes of morning rainfall maximum associated with deep cumulus convections in the western Pacific ocean and suggested that the tropospheric radiative cooling between the deep convective system and its surrounding cloud-free region is the main reason. Following Gray and Jacobson (1977), the influence of radiative heating/cooling on modulating the variation of $P_{\mathrm{SEC}}$ is examined through comparing the difference in temperature changes induced by the net radiation (denoted by $T^{\mathrm{R}}$) between SEC and SCS. The selection of SCS (dash boxed areas in Figure 4) is based on the fact that the moist air mass over SEC mainly comes from SCS during the summer months (Ding, 2004). In this study, $T^{\mathrm{R}}$ is obtained through the following equation:

$$T^{\mathrm{R}} = \int_{t-3h}^{t} \left[\frac{\partial \mathrm{T}^{\mathrm{SW}}}{\partial t} + \frac{\partial \mathrm{T}^{\mathrm{LW}}}{\partial t}\right] \mathrm{d}t \qquad (4)$$

where $(\partial T^{\mathrm{SW}}/\partial t)$ and $(\partial T^{\mathrm{LW}}/\partial t)$, which represent the temperature tendency due to shortwave and longwave radiation respectively, are directly extracted from the GEOS5 datasets. The 3-hourly anomalies, S1 and S2 harmonics of $T^{\mathrm{R}}$ area-averaged over SEC and SCS, are computed and results at four selected synoptic time steps [0300, 0900, 1500, and 2100 UTC, including times of S1($T^{\mathrm{R}}$) and S2($T^{\mathrm{R}}$) peaks, are shown in Figure 5.

Previous studies indicated that the land–sea differential radiative heating/cooling has a significant implication in modulating the diurnal rainfall variation over SEC (e.g. Ramage, 1952). As seen in Figure 5(a), the difference in $\Delta(T^{\mathrm{R}})$ between SEC and SCS [hereafter, $\Delta(T^{\mathrm{R}})_{\mathrm{SEC-SCS}}$] reaches its maximum value at 0900 UTC because land is

 

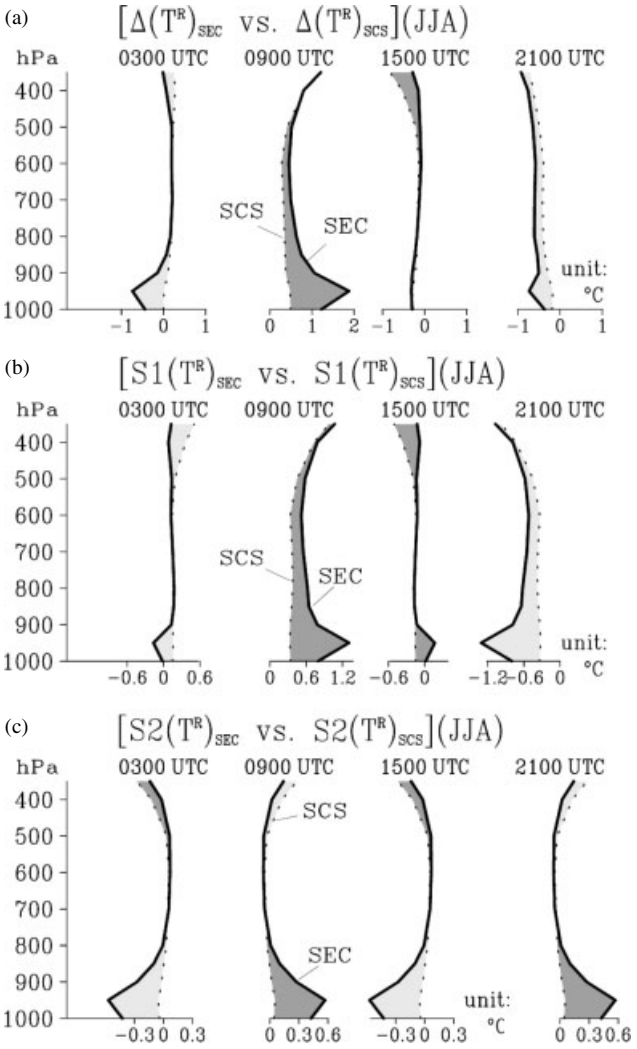


**Figure 5.** JJA mean of (a) anomalies, (b) diurnal harmonic, and (c) semi-diurnal harmonic of temperature changes induced by net radiative heating/cooling, i.e. $T^{\mathrm{R}}$, area-averaged over SEC (solid line) and over SCS (dotted line) at 0300, 0900, 1500, and 2100 UTC. The domain of SEC and SCS is denoted by boxed areas in Figure 4. The dark-grey areas in (a)–(c) indicate that the variation of $(T^{\mathrm{R}})_{\mathrm{SEC}}$ is larger than $(T^{\mathrm{R}})_{\mathrm{SCS}}$, whereas the light-grey areas indicate that the former is smaller than the latter. The unit of $T^{\mathrm{R}}$ is°C.

heating faster than sea during the daytime. About 75% of the low-level land–sea differential radiative heating, in terms of $\Delta[T^{\mathrm{R}}\ (925\ \mathrm{hPa})]_{\mathrm{SEC-SCS}}$, at 0900 UTC is attributed to its S1 component (Figure 5(b)), close to the percentage of $\mathrm{S1}(P)_{\mathrm{SEC}}$ in explaining the variation of $\Delta(P)_{\mathrm{SEC}}$ at the same time step (Figure 2(c)). Because a larger vertical decreasing rate of $\mathrm{S1}(T^{\mathrm{R}})$ between 925 and 850 hPa is revealed at 0900 UTC over SEC than SCS (Figure 5(b)), a larger thermal instability with more ascending motion is likely to be observed over SEC in the afternoon. This implication is verified in Figure 3(c), showing that the magnitude of the S1 harmonics of low-level wind convergence and precipitation at 0900 UTC over SEC is much larger than those over SCS.

In contrast to the temporal evolution of $\mathrm{S1}(T^{\mathrm{R}})_{\mathrm{SEC-SCS}}$, it is noted from Figure 5(c) that the low-level $\mathrm{S2}(T^{\mathrm{R}})_{\mathrm{SEC}}$ is warmer than $\mathrm{S2}(T^{\mathrm{R}})_{\mathrm{SCS}}$ at both 0900 and 2100 UTC. Such a low-level thermal gradient between SEC and SCS likely leads to a circulation with upward motions over SEC and downward motions over SCS and, in turn, forms an $\mathrm{S2}(P)_{\mathrm{SEC}}$ peak at 0900 and 2100 UTC. This inference is examined further based on the horizontal distribution of $\mathrm{S2}(P)$ at 2100 UTC (Figure 6(a)). It is noted from Figure 6(a) that a larger amount of $\mathrm{S2}(P)$ is observed over SEC than over SCS, suggesting that the local convection is much deeper over SEC than over SCS. Other evidence for supporting that change in $\mathrm{S2}(T^{\mathrm{R}})$ can induce a relatively unstable environment over SEC than over SCS at 2100 UTC is revealed from a comparison between the thermal instability induced by the vertical differential $\mathrm{S2}(T^{\mathrm{R}})_{\mathrm{SEC}}$ (i.e. $\mathrm{S2}(\partial T^{\mathrm{R}}/\partial p)_{\mathrm{SEC}}$, where $p$ is pressure) and vertical differential $\mathrm{S2}(T^{\mathrm{R}})_{\mathrm{SCS}}$ (i.e. $\mathrm{S2}(\partial T^{\mathrm{R}}/\partial p)_{\mathrm{SCS}}$). In general, a greater infrared cooling at the cloud top than at the cloud base can result in destabilization of the atmosphere (Lau *et al.*, 1998). In other words, a larger magnitude of $\mathrm{S2}(\partial T^{\mathrm{R}}/\partial p)$ would imply a more unstable environment. According to Figure 5(c), the magnitude of $\mathrm{S2}(\partial T^{\mathrm{R}}/\partial p)$ at 2100 UTC for the difference between upper level (e.g. 300 hPa) and lower level (e.g. 925 hPa) is larger over SEC than over SCS, confirming that SEC is relatively unstable compared to SCS at 2100 UTC.

Note that, consistent with the difference between $\mathrm{S1}(P)_{\mathrm{SEC}}$ and $\mathrm{S2}(P)_{\mathrm{SEC}}$ (see Figure 2(c)), the magnitude of $\mathrm{S2}(T^{\mathrm{R}})_{\mathrm{SEC-SCS}}$ is also about half that of $\mathrm{S1}(T^{\mathrm{R}})_{\mathrm{SEC-SCS}}$. It is shown in Figure 2(c) that, even though the magnitude of $\mathrm{S2}(P)_{\mathrm{SEC}}$ is smaller than $\mathrm{S1}(P)_{\mathrm{SEC}}$, the evolution of $\mathrm{S2}(P)_{\mathrm{SEC}}$ prevents the rainfall decreasing from $\mathrm{S1}(P)_{\mathrm{SEC}}$ and contributes most to a relative increase in rainfall at 0500 h/2100 UTC. On the other hand, it should be also noted that much of the change in radiative heating/cooling might occur as a result of increased (relatively) convection in the early morning over SEC that is originally driven by thermal advection. Because the change in radiative heating/cooling would likely encourage relatively more convection, there might be a positive radiative–convection feedback over SEC. A crucial part of this mechanism occurring at night is the lack of solar absorption to offset cloud top cooling.

Finally, to complete the examination of hydrological cycle–radiation interaction, we explain the maintenance of rainfall variation by diagnosing the following water vapor budget equation:

$$P = E + (-\nabla \cdot \mathbf{Q}) + \left(-\frac{\partial W}{\partial t}\right) \tag{5}$$

where $W$, $\nabla \cdot \mathbf{Q}$, $P$ and $E$ are respectively total precipitable water, convergence/divergence of the vertical-integrated vapor flux, precipitation and evaporation. Chen (2005) suggested that rainfall over EA is maintained by the water vapor supply through the convergence of water vapor flux (i.e. $P \sim (-\nabla \cdot \mathbf{Q})$]. Huang *et al.* (2010) examined the S1 harmonic of hydrological circulation over SEC and indicated further that the amplitude of $\mathrm{S1}(P)_{\mathrm{SEC}}$ and $\mathrm{S1}(-\nabla \cdot \mathbf{Q})_{\mathrm{SEC}}$ is about one order larger than the amplitude of $\mathrm{S1}(E)_{\mathrm{SEC}}$ and $\mathrm{S1}(-\partial W/\partial t)_{\mathrm{SEC}}$. In addition, because the correlation coefficient (hereafter, $\sigma$) between the temporal variation of $\mathrm{S1(P)}_{\mathrm{SEC}}$ and $\mathrm{S1}(-\nabla \cdot \mathbf{Q})_{\mathrm{SEC}}$ is very high (i.e. $\sigma \sim 0.94$ in summer), it has been suggested that the evolution of $\mathrm{S1}(P)_{\mathrm{SEC}}$ follows that of $\mathrm{S1}(-\nabla \cdot \mathbf{Q})_{\mathrm{SEC}}$ (Huang *et al.*, 2010). In this study, we focus on how $\mathrm{S2}(P)_{\mathrm{SEC}}$, i.e. the important factor for the formation of the early-morning rainfall peak over SEC, is maintained. It is noted that the temporal evolution of $\mathrm{S2}(P)_{\mathrm{SEC}}$ (Figure 2(c)) follows that of $\mathrm{S2}(-\nabla \cdot \mathbf{Q})_{\mathrm{SEC}}$ (Figure 6(c)), suggesting that they are closely related to each other ($\sigma \sim 0.91$). As seen from Figure 6(b), $\mathrm{S2}(-\nabla \cdot \mathbf{Q})_{\mathrm{SEC}}$ contributes much more than

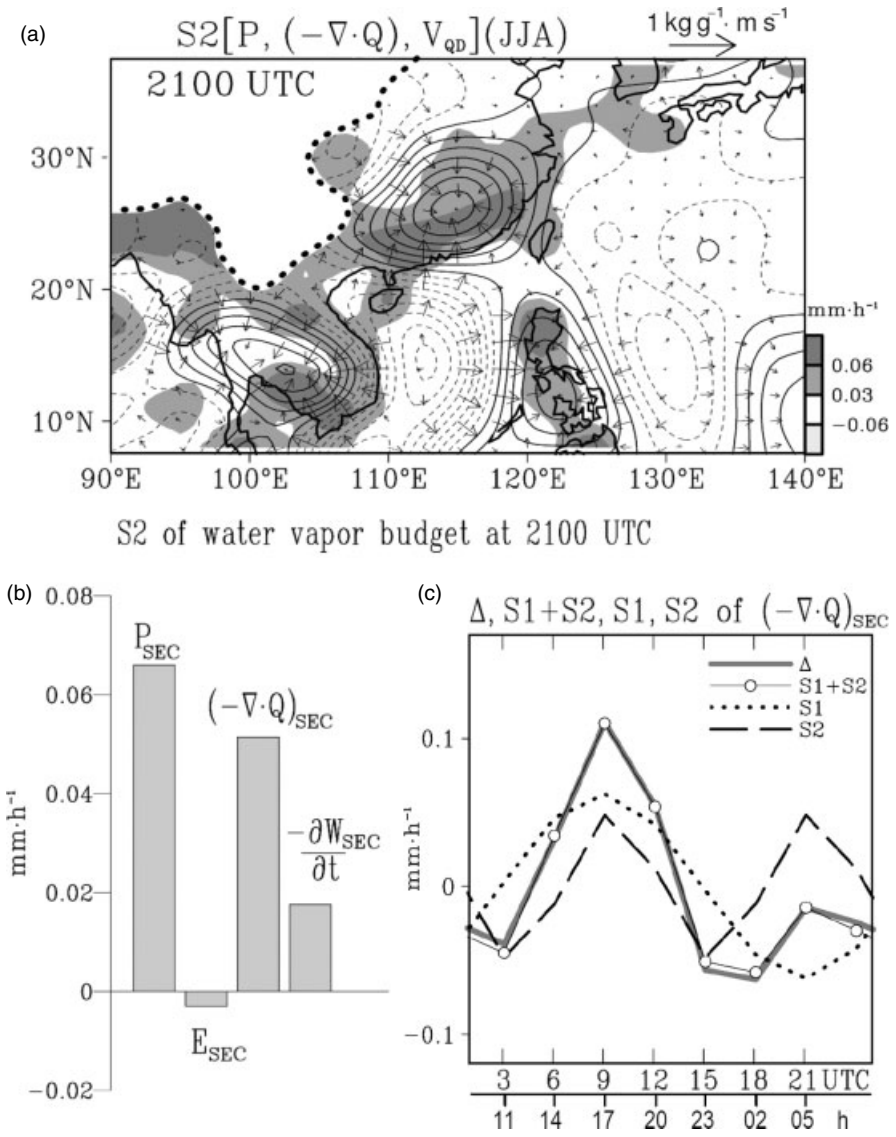


**Figure 6.** (a) JJA mean of S2($P$) (shaded) superimposed with the S2 harmonic (contours) of convergence of water vapor flux ($-\nabla \cdot \mathbf{Q}$) at 2100 UTC (0500 h). The color scale of (a) is shown at bottom right. Vectors of convergence of water vapor flux are added in (a). The contour interval of S2($-\nabla \cdot \mathbf{Q}$) is $2 \times 10^{-2}$ mm h$^{-1}$. (b) Water vapor budget analysis for the maintenance of S2$(P)_{\mathrm{SEC}}$ at 2100 UTC. (c) Similar to Figure 2(c), but for the temporal variations of $(-\nabla \cdot \mathbf{Q})_{\mathrm{SEC}}$.

S2$(-\partial W/\partial t)_{\mathrm{SEC}}$ and S2$(E)_{\mathrm{SEC}}$ to the maintenance of S2$(P)_{\mathrm{SEC}}$ at 2100 UTC. Most importantly, it is found that the S2 harmonic of hydrological circulation, which shows the water vapor transporting from SCS to SEC in the early morning (Figure 6(c)), is in response to the S2 harmonic of land–sea differential radiative heating/cooling between SEC and SCS (Figure 5(c)), as discussed earlier.

## 6. Conclusion

During the summer months, the diurnal rainfall variation over SEC frequently consists of a major peak at 1700 h (i.e. 0900 UTC) and a minor peak at 0500 h (i.e. 2100 UTC). In this study, we note that the variation of S1$(P)_{\mathrm{SEC}}$ determines the time of the occurrence of afternoon rainfall peak over SEC, whereas the variation of S2$(P)_{\mathrm{SEC}}$ controls the occurrence of early-morning rainfall peak over SEC. Analyses of various datasets have been performed to identify the possible mechanisms for the establishment of this early-morning maximum. The results are depicted in Figure 7 and summarized below.

A diagnosis of the atmospheric heat budget indicates that the air is flowing from the warmer SCS to the cooler SEC at late night (i.e. 0200 h/1800 UTC), which tends to increase the low-level atmospheric temperature over SEC in the early morning (i.e. 0500 h/2100 UTC). Such a low-level thermal advection warming is generally coupled with an upper-level thermal advection cooling (item 1 in Figure 7) and, in turn, reduces the atmospheric thermal stability in the early morning over SEC. In addition to the diurnally varying vertical differential thermal advection, we find that the land–sea difference of the S2 harmonic of radiative heating/cooling between SEC and SCS (item 2 in Figure 7) is another important factor for increasing the early-morning thermal instability. Computation of the S2 harmonic of water vapor budget further suggests that the early-morning rainfall over SEC is mainly maintained by the convergence of water vapor flux transporting from SCS to SEC (item 3 in Figure 7). Among these three mechanisms (items 1–3), thermal advection can be seen as the main driving mechanism for the early-morning peak in rainfall and the other two mechanisms can be seen as subsequent positive

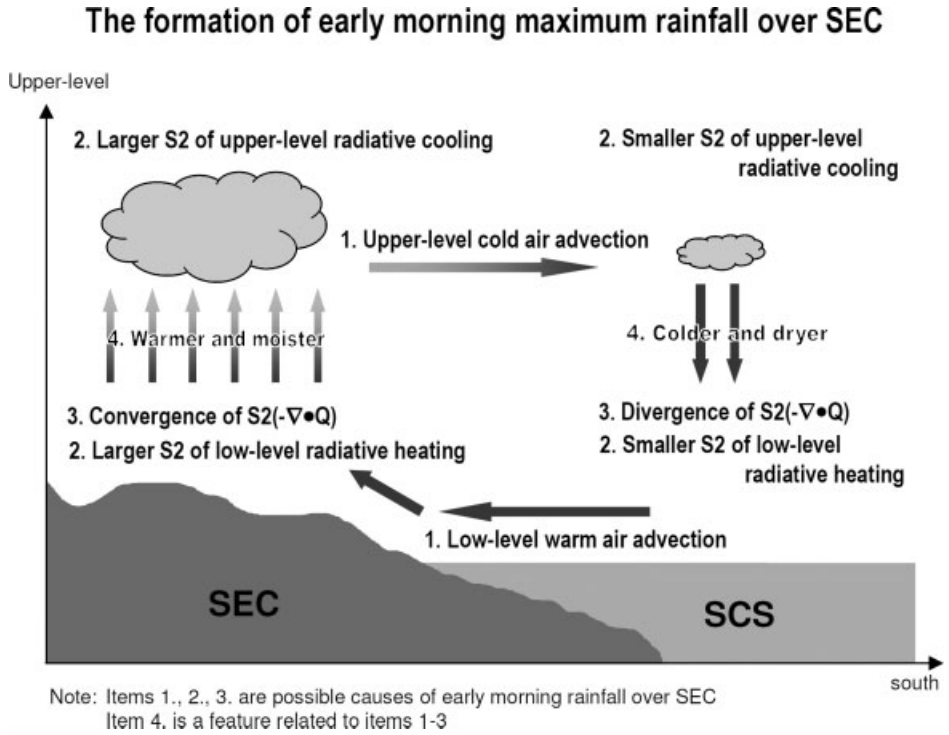


**Figure 7.** Schematic diagram illustrating the formation of early-morning maximum rainfall over SEC induced by the late-night vertical differential thermal advection (item 1), S2 harmonic of land–sea differential radiation heating/cooling between SEC and SCS (item 2), and S2 harmonic of land–sea differential water vapor flux convergence/divergence between SEC and SCS (item 3). Modulated by these three mechanisms, the atmospheric temperature above SEC at 0500 h/2100 UTC is relatively unstable compared to other hours without solar heating (item 4). These relatively unstable atmospheric conditions correspond to the maximum value of S2($P$) over SEC in the early morning.

feedback mechanisms which occur as a result of the initial increase in convective instability (or reduction in stability) over SEC. Modulated by these three mechanisms, the atmospheric air above SEC is relatively unstable at 2100 UTC compared with other times without solar heating and, in turn, leads to a minor rainfall peak at 2100 UTC. Because the diurnal rainfall over SEC varies seasonally (Li *et al.*, 2008), a future study is necessary to clarify whether our proposed mechanisms have any seasonal difference.

## Acknowledgements

We thank two anonymous reviewers for their comments and suggestions, which greatly improved the manuscript. The GEOS5 data used were provided by NASA Goddard Space Flight Center. The TRMM data were obtained from the NASA Tropical Rainfall Measuring Mission.

## References

Asai T, Ke S, Kodama Y. 1998. Diurnal variability of cloudiness over East Asia and the Western Pacific Ocean as revealed by GMS during the warm season. *J. Meteorol. Soc. Jpn* **76**: 675–684.

Chan JCL, Ng MH. 1993. Morning showers over Hong Kong during summer. *Bull. Hong Kong Meteorol. Soc.* **3**: 14–25.

Chen G, Sha W, Iwasaki T. 2009. Diurnal variation of precipitation over southeastern China: spatial distribution and its seasonality. *J. Geophys. Res.* **114**: D13103, DOI: 10.1029/2008JD011103.

Chen H, Yu R, Li J, Yuan W, Zhou T. 2010. Why nocturnal long-duration rainfall presents an eastward delayed diurnal phase along the Yangtze River. *J. Climate* **23**: 905–917.

Chen TC. 2005. Variation of the Asian monsoon water vapor budget: interaction with the global-scale modes. In *Asian Monsoon*, Wang B (ed.) 417–458. Springer: Berlin.

Chen TC, Yen MC, Hsieh JC, Arritt RW. 1999. Diurnal and seasonal variations of the rainfall measured by the automatic rainfall and meteorological telemetry system in Taiwan. *Bull. Am. Meteorol. Soc.* **80**: 2299–2312.

Dai A. 2001. Global precipitation and thunderstorm frequencies. Part II: Diurnal variations. *J. Climate* **14**: 1112–1128.

Dai A, Deser C. 1999. Diurnal and semidiurnal variations in global surface wind and divergence fields. *J. Geophys. Res.* **104**: 31109–31125.

Deser C, Smith CA. 1998. Diurnal and semidiurnal variations of the surface wind field over the tropical Pacific Ocean. *J. Climate* **11**: 1730–1748.

Ding YH. 2004. Seasonal march of the East-Asian summer monsoon. In *East Asian Monsoon. World Scientific Series on Meteorology of East Asia*, Vol. 2, Chang CP (ed.) 3–53. World Scientific Publishing: Singapore.

Gray WM, Jacobson RW. 1977. Diurnal variation of deep cumulus convection, *Mon. Weather Rev.* **105**: 1171–1188.

Haddad ZS, Smith EA, Kummerow CD, Iguchi T, Farrar MR, Durden SL, Alves M, Olson WS. 1997a. The TRMM 'Day-1' radar/radiometer combined rain-profiling algorithm. *J. Meteorol. Soc. Jpn* **75**: 799–809.

Haddad ZS, Short DA, Durden SL, Im E, Hensley S, Grable MB, Black RA. 1997b. A new parametrization of the rain drop size distribution. *IEEE Trans. Geosci. Remote Sens.* **35**: 532–539.

Hamilton K. 1980. The geographical distribution of the solar semidiurnal surface pressure oscillation. *J. Geophys. Res.* **85**: 1945–1949.

Holton JR. 1992. *An Introduction to Dynamic Meteorology*. Academic Press: New York.

Hong Y, Hsu KL, Sorooshian S, Gao X. 2005. Improved representation of diurnal variability of rainfall retrieved from the Tropical Rainfall Measurement Mission Microwave Imager adjusted Precipitation estimation from Remotely Sensed Information Using Artificial Neural Networks (PERSIANN) system. *J. Geophys. Res.* **110**: D06102, DOI: 10.1029/2004JD005301.

Huang WR, Chan JCL, Wang SY. 2010. A planetary-scale land-sea breeze circulation in East Asia and the western North Pacific. *Q. J. R. Meteorol. Soc.* **136**: 1543–1553.

Kikuchi K, Wang B. 2008. Diurnal precipitation regimes in the global tropics. *J. Climate* **21**: 2680–2696.

Lau KM, Ho CH, Kang IS. 1998. Anomalous atmospheric hydrologic processes associated with ENSO: mechanisms of hydrologic cycle–radiation interaction. *J. Climate* **11**: 800–815.

Li J, Yu R, Zhou T. 2008. Seasonal variation of the diurnal cycle of rainfall in southern contiguous China. *J. Climate* **21**: 6036–6043.

Peacock JE. 1952. *Hong Kong Meteorological Records and Climatological Notes, Technical Notes Memoir No. 5*. Royal Observatory, Hong Kong.

 

Ramage CS. 1952. Diurnal variation of summer rainfall over east China, Korea and Japan. *J. Atmos. Sci.* **9**: 83–86.
Rienecker MM, Suarez MJ, Todling R, Bacmeister J, Takacs L, Liu HC, Gu W, Sienkiewicz M, Koster RD, Gelaro R, Stajner I, Nielsen JE. 2008. The GEOS-5 Data Assimilation System: Documentation of Versions 5.0.1, 5.1.0, and 5.2.0. *Technical Report Series on Global Modeling and Data Assimilation*, 27.
Simpson JS, Kummerow C, Tao WK, Adler RF. 1996. On the Tropical Rainfall Measuring Mission (TRMM). *Meteorol. Atmos. Phys.* **60**: 19–36.
Wai MMK, Welsh PT, Ma WM. 1996. Interaction of secondary circulations with the summer monsoon and diurnal rainfall over Hong Kong. *Bound. Layer Meteorol.* **81**: 123–146.
Wallace JM, Hartranft FR. 1969. Diurnal wind variations, surface to 30 kilometers. *Mon. Weather Rev.* **97**: 446–455.
Wang CC, Chen GTJ, Carbone RE. 2004. A climatology of warm-season cloud patterns over east Asia based on GMS infrared brightness temperature observations. *Mon. Weather Rev.* **132**: 1606–1629.
Wei MY, Johnson DR, Townsend RD. 1983. Seasonal distributions of diabatic heating during the First GARP Global Experiment. *Tellus* **35A**: 241–255.
Yang S, Smith EA. 2006. Mechanisms for diurnal variability of global tropical rainfall observed from TRMM. *J. Climate* **19**: 5190–5226.
Yin S, Chen D, Xie Y. 2009. Diurnal variations of precipitation during the warm season over China. *Int. J. Climatol.* **29**: 1154–1170.
Yu R, Zhou T, Xiong A, Zhu Y, Li J. 2007a. Diurnal variations of summer precipitation over contiguous China. *Geophys. Res. Lett.* **34**: L01704, DOI: 10.1029/2006GL028129.
Yu R, Xu Y, Zhou T, Li J. 2007b. Relation between rainfall duration and diurnal variation in the warm season precipitation over central eastern China. *Geophys. Res. Lett.* **34**: L13703, DOI: 10.1029/2007GL030315.
Yu R, Li J, Chen H. 2009. Diurnal variation of surface wind over central eastern China. *Clim. Dyn.* **33**: 1089–1097.
Zhou W, Chan JCL. 2005. Intraseasonal oscillations and the South China Sea summer monsoon onset. *Int. J. Climatol.* **25**: 1585–1609.
Zhao Z, Leung LR, Qian Y. 2005. Characteristics of diurnal variations of precipitation in China for the recent years. *CLIVAR Exchanges, No. 3*, 24–26. International CLIVAR Project Office, Southampton, UK.
Zhou T, Yu R, Chen H, Dai A, Pan Y. 2008. Summer precipitation frequency, intensity, and diurnal cycle over China: a comparison of satellite data with rain gauge observations. *J. Climate* **21**: 3997–4010.

 